

## Composite Nafion/Sulfated Zirconia Membranes: Effect of the Filler Surface Properties on Proton Transport Characteristics<sup>†</sup>

Alessandra D'Epifanio,<sup>‡,§</sup> Maria Assunta Navarra,<sup>§</sup> F. Christoph Weise,<sup>‡</sup>  
Barbara Mecheri,<sup>§</sup> Jaime Farrington,<sup>‡</sup> Silvia Licoccia,<sup>§</sup> and Steve Greenbaum<sup>\*‡</sup>

<sup>‡</sup>Hunter College of the City University of New York, New York, New York 10065, <sup>§</sup>Department of Chemical Science and Technology, University of Rome "Tor Vergata", Via della Ricerca Scientifica, 1-00133 Roma, Italy, and <sup>§</sup>Department of Chemistry, University of Rome "La Sapienza", P.le Aldo Moro 5-00185 Roma, Italy

Received May 30, 2009. Revised Manuscript Received October 29, 2009

Because of their strong acidity and water affinity, sulfated zirconia nanoparticles were evaluated as inorganic additives in the formation of composite Nafion-based membranes. Two types of sulfated zirconia were obtained according to the preparation experimental conditions. Sulfated zirconia-doped Nafion membranes were prepared by a casting procedure. The properties of the composite membranes were compared with those of an unfilled Nafion membrane obtained by the same preparation method. The water uptake, measured at room temperature in a wide relative humidity range, was higher for the composite membranes, this confirming the hydrophilic nature of the selected additives. The membrane doped by zirconia particles having the highest sulfate group concentration showed the highest water diffusion coefficient in the whole range of temperature and relative humidity investigated because of the presence of  $\text{SO}_4^{2-}$  providing extra acid sites for water diffusion. The proton diffusivity calculated from impedance spectroscopy measurements was compared with water self-diffusion coefficients measured by NMR spectroscopy. The difference between proton and water diffusivity became significant only at high humidification levels, highlighting the role of water in the intermolecular proton transfer mechanism. Finally, great improvements were found when using the composite membrane as electrolyte in a fuel cell working at very low relative humidity.

### 1. Introduction

Metal oxides have been extensively investigated as inorganic additives in proton conducting membranes used as ionic separators in polymer electrolyte membrane fuel cells (PEMFCs).<sup>1–3</sup> It was demonstrated that the addition of metal oxides, in the form of nano- or sub-micrometric particles, improves the water retention and the thermomechanical stability of the membranes.<sup>4</sup> The properties of the state-of-the-art membranes (i.e., per-fluorosulphonic, Nafion-type, membranes) are, in fact, strictly dependent on their hydration level. This limits the operation temperature and imposes strict humidification requirements in the fuel cell devices.

In the research of higher-temperature proton-exchange membrane with adequate performances at low relative humidity (RH), various compounds, such as  $\text{SiO}_2$ ,  $\text{TiO}_2$ ,

and  $\text{ZrO}_2$ , have been added to a Nafion matrix.<sup>5–10</sup> This concept was suggested by Watanabe and co-workers and allowed cell operation at 80 °C under extremely dry conditions.<sup>11,1</sup> Moreover, depending on the degree of hydration, many oxides become good proton conductors. Hydrated tin dioxide, for example, exhibits high conductivity at a relatively low humidity, being one of the most effective compounds in retaining water.<sup>12</sup> Recently, the addition of  $\text{SnO}_2$  nanopowders to polymer electrolyte membranes was found to be extremely beneficial under operating cell condition of 120 °C and low RH.<sup>13–15</sup>

The use of inorganic proton conductors has been further explored. Costamagna et al. studied Nafion/zirconium

<sup>†</sup> Accepted as part of the 2010 "Materials Chemistry of Energy Conversion Special Issue".

<sup>\*</sup>Corresponding author.

- (1) Watanabe, M.; Uchida, H.; Seki, Y.; Emori, M.; Stonehart, P. *J. Electrochem. Soc.* **1996**, *143*, 3847–3852.
- (2) Adjemian, K. T.; Lee, S. J.; Srinivasan, S.; Benziger, J.; Bocarsly, A. *J. Electrochem. Soc.* **2002**, *149*, A256–A261.
- (3) Jalani, N. H.; Dunn, K.; Datta, R. *Electrochim. Acta* **2005**, *51*, 553–560.
- (4) Savadogo, O. *J. Power Sources* **2004**, *127*, 135–161.
- (5) Herring, A. M. *Polym. Rev.* **2006**, *46*, 245.
- (6) Sahu, A. K.; Selvarani, G.; Pitchumani, S.; Sridhar, P.; Shukla, A. K. *J. Electrochem. Soc.* **2007**, *154*, B123.

- (7) Baglio, V.; Di Blasi, A.; Aricò, A. S.; Antonucci, V.; Antonucci, P. L.; Serraino Fiory, F.; Licoccia, S.; Traversa, E. *J. New Mater. Electrochem. Syst.* **2004**, *7*, 275.
- (8) Chalkova, E.; Fedkin, M. V.; Wesolowski, D. J.; Lvov, S. *J. Electrochem. Soc.* **2005**, *152*, A1742.
- (9) Saccà, A.; Carbone, A.; Passalacqua, E.; D'Epifanio, A.; Licoccia, S.; Traversa, E.; Sala, E.; Traini, F.; Ornelas, R. *J. Power Sources* **2005**, *152*, 16–21.
- (10) Licoccia, S.; Traversa, E. *J. Power Sources* **2006**, *159*, 12.
- (11) Watanabe, M. U.S. Patent 5,472,799, **1995**.
- (12) Hara, S.; Takano, S.; Miyayama, M. *J. Phys. Chem. B* **2004**, *108*, 5634.
- (13) Abbaraju, R. R.; Dasgupta, N.; Virkar, A. V. *J. Electrochem. Soc.* **2008**, *155*, B1307–B1313.
- (14) Mecheri, B.; D'Epifanio, A.; Traversa, E.; Licoccia, S. *J. Power Sources* **2008**, *178*, 554–560.
- (15) Mecheri, B.; D'Epifanio, A.; Pisani, L.; Chen, F.; Traversa, E.; Weise, F. C.; Greenbaum, S.; Licoccia, S. *Fuel Cells* **2009**, in press.

phosphate membranes in cells working at high temperature. Their composite membranes showed stable behavior over time when maintained at 130 °C, while irreversible degradation affected unmodified Nafion under the same conditions<sup>16</sup>. Similarly, Alberti and co-workers proved that the addition of 10 wt % zirconium phosphate increases the stability of conductivity up to 140 °C at 90% RH with respect to undoped recast Nafion<sup>17</sup>.

Other types of very interesting compounds, to be effectively used as membrane additives, consists of solid electrolytes such as heteropolyacids (HPAs)<sup>18</sup>. Their conductivity is of the same order of magnitude as that of mineral acids, around 0.02–0.1 S cm<sup>-1</sup>, at room temperature but the high affinity for polar media makes them easily soluble.<sup>19</sup> To overcome this limitation, HPAs have been modified by exchanging their protons with other cations<sup>20</sup> or by supporting them on high-surface-area oxides. For instance, phosphotungstic acid (PWA) added to hydrated ZrO<sub>2</sub> leads to a stable strongly acidic material having a Hammet acidity H<sub>0</sub> of -9.3.<sup>21</sup> Composite Nafion membranes, doped by zirconia-supported PWA, were tested by accelerated in situ aging measurements, showing a good electrochemical stability (more than 150 cycles at 90 °C in a cell fed by dry gases).<sup>22</sup>

Similarly to HPAs, the sulfated metal oxides have become subjects of intensive studies, they being more stable than other solid superacids. In general, the incorporation of inorganic solid acids in conventional Nafion-type membranes is of primary interest, having the dual function of improving water retention as well as providing additional acidic sites.<sup>23</sup> Currently, sulfated zirconia (SZrO<sub>2</sub>) is recognized as one of the strongest superacid among all known solids (H<sub>0</sub> < -16)<sup>24,25</sup>. It has been demonstrated that the proton conductivity of sulfated zirconia, as well as its surface and crystallographic properties, varies largely depending on the method of preparation, in particular on the thermal treatments.<sup>26,27</sup>

Our group has recently investigated the influence of both a commercial micrometric SZrO<sub>2</sub> powder and of an in-house sulfated submicrometric zirconia on Nafion

properties.<sup>28,29</sup> Comparing composite SZrO<sub>2</sub>-doped membranes with unmodified Nafion membranes, a general enhancement was revealed in the fuel cell response, both in terms of power density delivered and of ohmic resistance. Moreover, the high-temperature impedance response of the SZrO<sub>2</sub>-doped Nafion-based cell was highly improved, showing a well-controlled charge-transfer resistance.<sup>30</sup>

We have now extended our study by evaluating the role of optimized sulfated zirconia particles. Thus, we synthesized and characterized two different types of SZrO<sub>2</sub> nanopowders having well-defined surface properties. Their use as additives in Nafion membranes will also be discussed. In addition to characterization of the new materials, we present evidence of a hopping proton transport mechanism associated with the presence of the nanoparticle surfaces.

## 2. Experimental Section

**2.1. Materials.** **2.1.1. Preparation of Sulfated Zirconia SZrO<sub>2</sub>.** Zirconium oxide was prepared by sol-gel<sup>31,32</sup> using zirconium *n*-propoxide Zr(*n*-PrO)<sub>4</sub>, (70 wt % in 1-propanol, Aldrich) and 1-propanol (99% Aldrich) as starting materials. The alkoxide precursor (Zr(*n*-PrO)<sub>4</sub>) was added dropwise, under a N<sub>2</sub> atmosphere, to a solution of 1-propanol/water 1:1 v/v under rapid stirring. The suspension obtained was stirred at room temperature for 1 h, then the solvent was evaporated under a vacuum at room temperature. The residual solid was divided in two portions for different thermal treatments. The first portion was dried at 110 °C for 15 h; the second one was dried at 110 °C for 15 h and then to 700 °C for 6 h. These samples will be labeled in the text as ZrO<sub>2</sub>(t) and ZrO<sub>2</sub>(t,m), respectively.

According to the work of Arata,<sup>33</sup> sulfonated-zirconia (SZrO<sub>2</sub>) was obtained using sulfuric acid as sulfating agent. ZrO<sub>2</sub>(t) and ZrO<sub>2</sub>(t,m) samples were stirred in H<sub>2</sub>SO<sub>4</sub> 0.5 M for 30 min at room temperature. The suspensions were decanted overnight and the liquid phase was removed. The obtained powders were dried at 110 °C for 2 h and then heated to 620 °C for 3 h.<sup>23,26</sup>

**2.1.2. Preparation of Membranes.** Nafion membranes, both with and without the inorganic additive, were prepared following a solution casting procedure. Accordingly, solvents of a Nafion solution (5 wt % in water and alcohols, Ion Power, Inc. E.W.1100) were gradually replaced by *N,N*-dimethylacetamide. When required, SZrO<sub>2</sub> powder was added in the amount of 5% with respect to the dry Nafion weight and homogeneously dispersed by vigorous stirring. The mixture was poured on a Petri dish and the solvent evaporated. A dry membrane was obtained and hot-pressed at 175 °C and 20 atm to improve the thermo-mechanical stability of the film. The membrane was finally purified and activated by subsequent immersions in boiling hydrogen peroxide (3 vol %), sulfuric acid (0.5 M) and deionized water. The membranes prepared, both doped and undoped, had a dry thickness ranging from 70 to 80 μm. Membranes containing SZrO<sub>2</sub>(t) and SZrO<sub>2</sub>(t,m) will be labeled

- (16) Costamagna, P.; Yang, C.; Bocarsly, A. B.; Srinivasa, S. *Electrochim. Acta* **2002**, *47*, 1023–1033.
- (17) Alberti, G.; Casciola, M.; Capitani, D.; Donnadio, A.; Narducci, R.; Pica, M.; Sganappa, M. *Electrochim. Acta* **2007**, *52*, 8125–8132.
- (18) Malhotra, S.; Datta, R. *J. Electrochem. Soc.* **1997**, *144*, L23.
- (19) Rao, P. M.; Wolfson, A.; Kababya, S.; Vega, S.; Landau, M. V. *J. Catal.* **2005**, *232*, 210.
- (20) Ramani, V.; Kunz, H. R.; Fenton, J. M. *Electrochim. Acta* **2005**, *50*, 1181.
- (21) Lopez-Salinas, E.; Hernandez-Cortez, J. G.; Cortez, M.; Navarrete, J.; Yanos, M.; Vazquez, A.; Armendaris, H.; Lopez, T. *Appl. Catal., A* **1998**, *175*, 43.
- (22) Saccà, A.; Carbone, A.; Pedicini, R.; Marrony, M.; Barrera, R.; Elomaa, M.; Passalacqua, E. *Fuel Cells* **2008**, *8*, 225–235.
- (23) Thampan, T. M.; Jalani, N. H.; Choi, P.; Datta, R. *J. Electrochem. Soc.* **2005**, *152*, A316–A325.
- (24) Misono, M.; Okuhara, T.; N, Mizuno *Successful Design of Catalysts*; Inui, T., Ed.; Elsevier: Amsterdam, 1988; p 267.
- (25) Yadav, G. D.; Nair, J. J. *Microporous Mesoporous Mater.* **1999**, *33*, 1.
- (26) Hara, S.; Miyayama, M. *Solid State Ionics* **2004**, *168*, 111–116.
- (27) Li, C.; Li, M. *J. Raman Spectrosc.* **2002**, *33*, 301–308.
- (28) Navarra, M. A.; Croce, F.; Scrosati, B. *J. Mater. Chem.* **2007**, *17*, 3210–3215.
- (29) Navarra, M. A.; Abbati, C.; Scrosati, B. *J. Power Sources* **2008**, *183*, 109–113.

- (30) Navarra, M.A.; Abbati, C.; Croce, F.; Scrosati, B. *Fuel Cells* **2009**, DOI: 10.1002/fuce.200800066.
- (31) Li, B.; Gonzalez, R. D. *Ind. Eng. Chem. Res.* **1996**, *35*, 3141–3148.
- (32) Licocchia, S.; Polini, R.; Cadia D'Ottavi, F.; Serraino Fiory, M.; Luisa Di Vona; Traversa, E. *J. Nanosci. Nanotechnol.* **2005**, *5*, 592–595.
- (33) Arata, K. *Appl. Catal., A* **1996**, *146*, 3–32.

in the text as N-SZrO<sub>2</sub>(t) and N-SZrO<sub>2</sub>(t,m) respectively. Undoped membranes, used as references in our comparative tests, will be referred to as “Nafion recast”.

**2.2. Methods.** X-ray diffraction (XRD) analysis of the samples was carried out by means of a Philips X-Pert Pro 500 diffractometer equipped with a Cu K $\alpha$  radiation source and graphite monochromator. To study the thermal property of the powders thermogravimetric analyses were performed by a TGA-DTA Netsch STA 419 or a TGA/SDTA 851 Mettler Toledo thermoanalyser.

The morphology and the average particle diameter were investigated by scanning electron microscopy (FE-SEM LEO model Supra 35).

**2.2.1. Water Uptake and Ion Exchange Capacity Measurement.** Water uptake (WU) was measured as a function of RH at room temperature. The samples were dried at 70 °C under vacuum for 24 h then weighed. They were equilibrated in a closed vessel at different relative humidity (RH) values by using saturated aqueous salt solutions: MgCl<sub>2</sub>, KCO<sub>3</sub>, KI, KCl, and H<sub>2</sub>O for achieving 33, 43, 69, 84 and 100% relative humidity, respectively. The amount of water adsorbed was evaluated after 15 days at each RH value. WU was calculated using the following equation

$$WU = \frac{W_{\text{swollen}} - W_{\text{dry}}}{W_{\text{swollen}}} \times 100 \quad (1)$$

where WU is expressed in percentage units,  $W_{\text{swollen}}$  is the weight of the membrane exposed to aqueous solutions, and  $W_{\text{dry}}$  is the weight of the dry membrane.

The ion exchange capacity (IEC) was determined by an acid–base titration with a potentiometric method. A typical amount of 50–100 mg of sample was dried overnight at 80 °C and then immersed in an appropriate amount of 0.1 M NaCl solution overnight at 65 °C under continuous stirring, so that H<sup>+</sup> of the polymer acid side chains could be replaced by Na<sup>+</sup>. The solution was then titrated with 0.1 M NaOH (Aldrich, volumetric standard). IEC values were calculated by the following equation

$$IEC = \frac{V_{\text{NaOH}} \times C_{\text{NaOH}}}{W_{\text{sample}}} \quad (2)$$

where IEC is the ion exchange capacity (meq g<sup>-1</sup>),  $V_{\text{NaOH}}$  the added titrant volume at the equivalent point (mL),  $C_{\text{NaOH}}$  is the molar concentration of the titrant,  $W_{\text{sample}}$  is the dry mass of the sample (g). It is generally understood that the drying procedure employed here and in most of the literature does not remove all of the water. But because all samples were treated the same and the titration results merely reflect the number of acid sites, the IEC values are unaffected by this residual water.

**2.2.2. Proton Conductivity.** The proton conductivity of the membranes was measured by electrochemical impedance spectroscopy (EIS) measurements using a Multichannel Potentiostat VMP3 (Princeton Applied 114 Research). An applied voltage of 20–40 mV and a frequency range of 500 kHz to 10 Hz were used. The membranes were sandwiched between commercial electrodes (E-Tek ELAT HT 140E-W with a platinum loading of 5 g<sup>-2</sup>) and the proton conductivity was measured in a homemade apparatus as a function of temperature by exposing the samples to saturated aqueous salt solutions, as described previously. RH values, determined by the use of different aqueous salt solutions, were assumed to be constant in the temperature range under investigation. Before measuring the proton conductivity, the

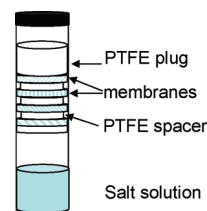


**Figure 1.** Sample configuration for PFGSE-NMR diffusion measurements.

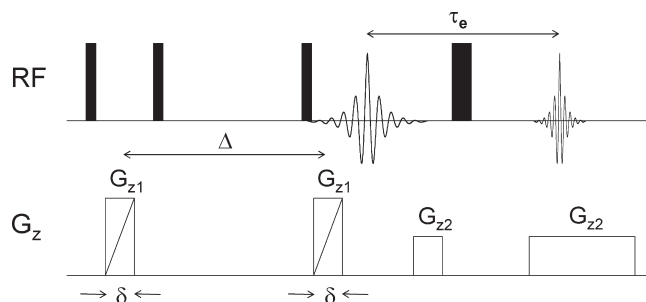


**Figure 2.** Diffusion-weighted single-axis NMR imaging sequence.

samples were equilibrated for 3 days at room temperature at each RH. The resistance of the membranes, hence their conductivity, was calculated fitting the impedance spectra in their linear portion. From the resistance values, we obtained the conductivity ( $\sigma$ ) value using the following equation:

$$\sigma = d/RA \quad (3)$$

where  $R$  is the resistance,  $d$  the distance between electrodes, and  $A$  is the electrode area.

**2.2.3. NMR Measurement.** For PFGSE-NMR diffusion measurements, samples of the dry membranes were cut into disks 4 mm in diameter and allowed to absorb water in a chamber maintained at constant RH until reaching equilibrium. The RH was controlled by exposure to a saturated salt solution as described previously. Once equilibrated, the membranes were stacked and sealed in a 5-mm NMR sample tube, with Teflon disks 3.5 mm in diameter and 1 mm thick serving as vertical partitions between different membranes. A 2 cm long glass insert half-filled with the same saturated salt solution used to equilibrate the membranes was placed below the stack to ensure a constant RH during the NMR experiments. Teflon slices were placed between the insert and the membranes to avoid capillary creep and contamination of the samples. The sample configuration is depicted in Figure 1. This relatively novel arrangement permits simultaneous evaluation of several membranes at once while ensuring that they all experience the same RH environment.<sup>34</sup> <sup>1</sup>H NMR imaging experiments were performed on a Chemagnetics system with a 7.2 T vertical wide bore magnet and a Nalorac z-spec single-axis gradient probe. The diffusion-weighted imaging pulse sequence illustrated in Figure 2 proved to be reliable. A stimulated echo (STE) block was used to encode diffusive displacements, and an image was obtained with a frequency-encoding gradient during acquisition of the spin echo generated by the  $\pi$  pulse. Frequency-encoding gradients were usually 14 G/cm. Typical parameters at 25 °C were  $G_{z1} = 7$ –109 G/cm, incremented in 15 steps,  $\delta = 3$  ms,  $\Delta = 20$  ms,  $\tau_e = 5$  ms, and eddy current delays of 2 ms following the gradient pulses.

(34) Fericola, A.; Weise, F. C.; Greenbaum, S. G.; Kagimoto, J.; Scrosati, B.; Soletto, A. *J. Electrochem. Soc.* **2009**, *156*, A514–A520.



To correct for variations in  $G_{z1}$  across the sample, we generated a map of the relative gradient amplitude at different positions along the gradient-coil axis using the diffusion-weighted imaging pulse sequence and a plug of doped water with known diffusivity at 25 °C of  $D_t = 2.3 \times 10^{-5} \text{ cm}^2 \text{ s}^{-1}$ . The actual gradient was calculated from the nominal values,  $G^*$ , of the applied gradient and the measured diffusivity,  $D^*(z)$ , as  $G_t(z)^2 = G^{*2} D^*(z) / D_t$ . The nominal position  $z$  was defined with respect to the center  $z_0$  of the gradient field as  $z - z_0 = (1/\gamma)(\delta\omega(z)/\delta G^*)$ , where  $\delta\omega(z)$  is the change in resonance frequency at nominal position  $z$  with an increase  $\delta G^*$  in the nominal gradient. During experiments with the stacked membranes, the nominal positions corresponding to peaks in the imaging spectrum of a sample were determined by the same approach employed with the water calibration sample. Once positions were known, correction factors were obtained from the gradient map by interpolation. From estimates of the uncertainties associated with the above procedure coupled with uncertainties in the standard PGSE method, as well as a limited number of repeated experiments, it was determined that the data is subject to a  $\pm 5\%$  variation.

**2.2.4. MEA Testing.** Fuel cell tests were performed by using a compact system (850C, Scribner Associates Inc.) connected to a 5 cm<sup>2</sup> cell fixture. The active surface of the used electrodes (E-Tek, 0.5 mg Pt cm<sup>-2</sup>) was brushed with a Nafion solution (ca. 0.4 mg dry Nafion cm<sup>-2</sup>). The membrane-electrode assembly, MEA, was realized by hot pressing the given membrane between two electrodes at 120 °C and 2 atm for 7 min. The cell was fed with H<sub>2</sub> and air according to current-dependent mass flow rates, by using an excess of the reactants amount required by the Faraday's law. Namely, the excess were: for the anode 1.4 and for the cathode 3.3 times those required from the reactions stoichiometry.

The humidification of the cell was accomplished by bubbling the fed gases through stainless steel cylinders incorporated in the compact system and containing distilled water. Reactant gas pressure in the cell could be varied by a back-pressure control module. The temperature of the humidifiers, as well as that of the cell, was properly set to achieve the desired relative humidity. The relative humidity values were calculated on the basis of water vapor pressure at cell temperature and at humidifier temperature<sup>35</sup>. Before recording polarization curves as a function of relative humidity, the cell was conditioned by fast current scans for two days at increasing temperature (from 30 to 99 °C) under full humidification.

### 3. Result and Discussion

#### 3.1. Characterization of ZrO<sub>2</sub> and SZrO<sub>2</sub> Samples.

Two Zirconia samples were prepared through a sol-gel procedure followed by two different thermal treatments. Figure 3 shows their TG-DTA profiles. The sample heated to 700 °C for 6 h, ZrO<sub>2</sub>(t,m), showed no weight losses in the whole range of temperature investigated (Figure 3a), whereas for the sample heated to 110 °C for 15 h, ZrO<sub>2</sub>(t), two weight losses were observed (Figure 3b). The first one (8 wt %), corresponding to a large endothermic peak in the DTA curve, was centered at a 140 °C, and it is due to desorption of water and propanol occluded in the gel. The second weight loss (2 wt %) was

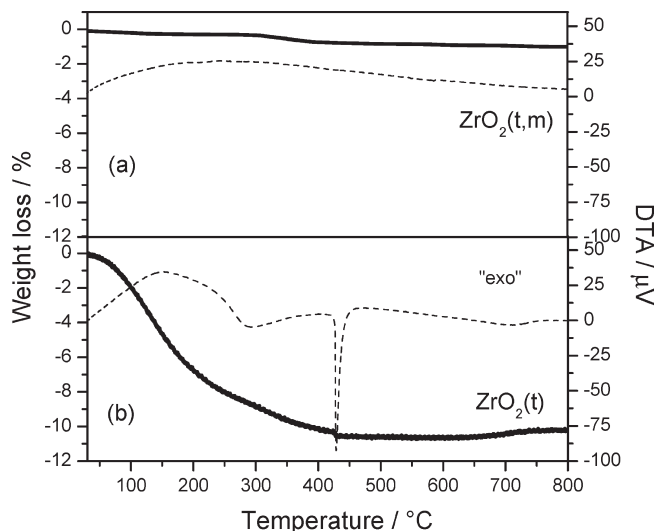


**Figure 3.** TG (solid line) and DTA (dashed line) responses of ZrO<sub>2</sub> precursor (a) calcined at 700 °C for 6 h and (b) dried at 110 °C for 15 h.

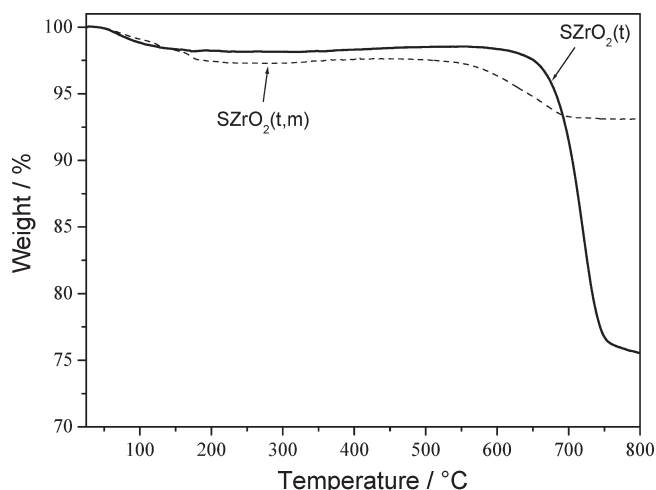


**Figure 4.** TG responses of SZrO<sub>2</sub>(t) (solid line) and SZrO<sub>2</sub>(t,m) (dashed line) powders.

associated with a DTA exothermic peak centered at 290 °C and can be related to the loss of residual organic groups and to the decomposition of zirconium hydroxide crystals, Zr(OH)<sub>4</sub>, into ZrO<sub>2</sub>.<sup>36</sup> The exothermal peak occurred at 430 °C and is attributed to the partial transformation from the amorphous quasi-tetragonal phase to monoclinic phase.

Figure 4 shows the thermogravimetric (TG) response of the sulfated-ZrO<sub>2</sub> samples. Both SZrO<sub>2</sub>(t,m) and SZrO<sub>2</sub>(t) samples showed a weight loss of about 2–3% at temperatures lower than 200 °C because of water evaporation. The second weight loss occurring at higher temperature, is attributed to the decomposition of SO<sub>4</sub><sup>2-</sup> bound to the surface of ZrO<sub>2</sub>, which leads to the formation of SO<sub>2</sub>. The decomposition of sulfate groups started at 550 °C for SZrO<sub>2</sub>(t,m) and at 650 °C for SZrO<sub>2</sub>(t) indicating a higher stability of the latter sample<sup>31</sup>. The higher weight loss observed for the SZrO<sub>2</sub>(t) sample

(35) Adjemian, K. T.; Dominey, R.; Krishnan, L.; Ota, H.; Majsztrik, P.; Zhang, T.; Mann, J.; Kirby, B.; Gatto, L.; Velo-Simpson, M.; Leahy, J.; Srinivasan, S.; Benziger, J. B.; Bocarsly, A. B. *Chem. Mater.* **2006**, *18*, 2238.

(36) Wang, J. A.; Valenzuela, M. A.; Salmones, J.; Vázquez, A.; García-Ruiz, A.; Bokhimi, X. *Catal. Today* **2001**, *68*, 21–30.

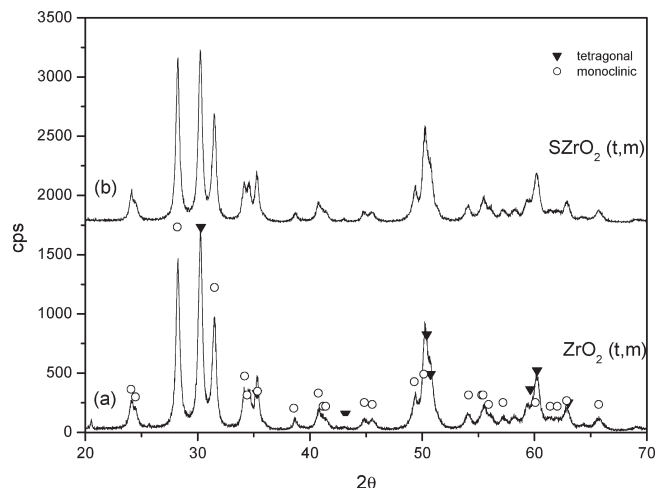


**Figure 5.** XRD patterns of the  $\text{ZrO}_2(\text{t})$  powder (a) before and (b) after the sulphating process.

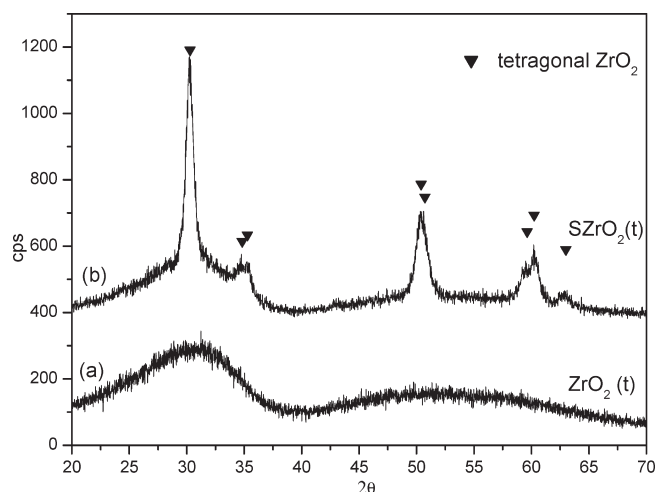


**Figure 6.** XRD patterns of the  $\text{ZrO}_2(\text{t,m})$  powder (a) before and (b) after the sulphating process.

(ca. 22%) with respect to that observed for the  $\text{SZrO}_2(\text{t,m})$  (ca. 4%) is indicative of its higher sulfate group content.

Figures 5 and 6 display the XRD patterns of the two samples before (Figures 5a, 6a) and after (Figures 5b, 6b) the sulphating process. It is not surprising that the two different thermal treatments led to different phases, in fact it is well-known that several factors, such as thermal treatments and the conditions for obtaining the oxide precursor, have been acknowledged to play a key role in affecting the phase of the  $\text{ZrO}_2$ .<sup>37</sup> The XRD patterns of the samples  $\text{ZrO}_2(\text{t,m})$  and  $\text{SZrO}_2(\text{t,m})$  show that tetragonal and monoclinic crystals coexisted before and after the sulphating procedure, see Figure 5. This finding indicates that, when sulfuric acid is added to the crystalline  $\text{ZrO}_2(\text{t,m})$  sample, the  $\text{SO}_4^{2-}$  groups bound to the oxide surface do not influence the structural phase composition. The XRD patterns of the  $\text{ZrO}_2(\text{t})$  and  $\text{SZrO}_2(\text{t})$  samples are displayed in Figure 6. XRD profile of

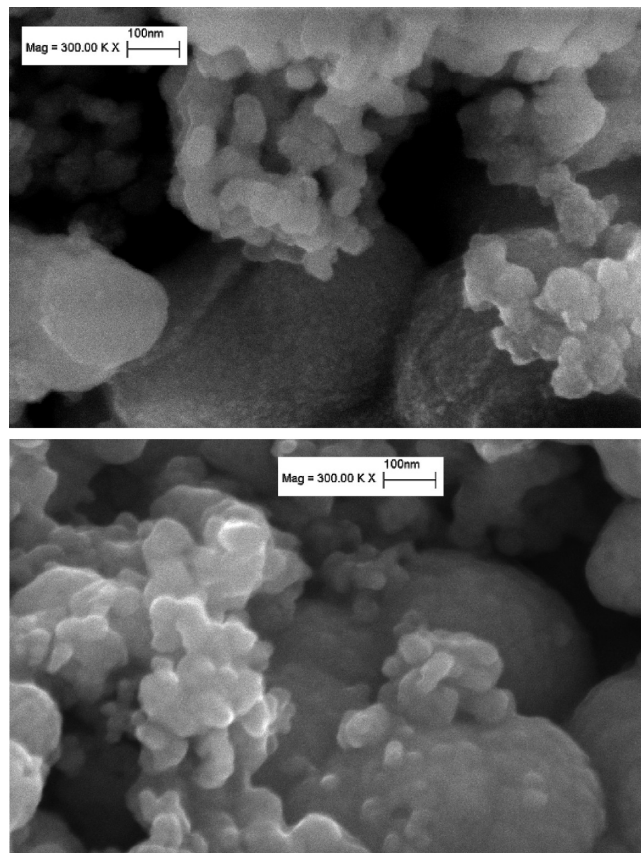


**Figure 7.** SEM images of (a)  $\text{SZrO}_2(\text{t})$  and (b)  $\text{SZrO}_2(\text{t,m})$  nano powders.

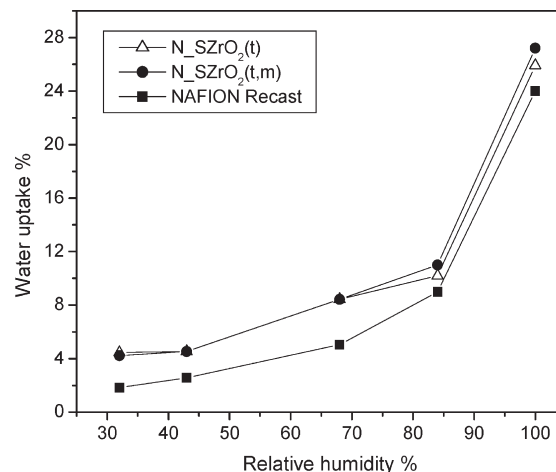


**Figure 8.** Water uptake vs RH for nanocomposite  $\text{N-SZrO}_2(\text{t})$ ,  $\text{N-SZrO}_2(\text{t,m})$ , and Nafion recast membranes at 25 °C.

unsulfated  $\text{ZrO}_2(\text{t})$  (Figure 6a) shows a nearly amorphous pattern, with traces of tetragonal zirconia microcrystals as indicated by the incipient peak at  $30.2 (2\theta)$ . After the sulphating process, a pure tetragonal phase was obtained (Figure 6b). The addition of a sulphating agent to amorphous  $\text{ZrO}_2$  is expected to cause substitution of the  $\text{OH}^-$  groups present on the zirconia surface by  $\text{SO}_4^{2-}$  ions leading to the stabilization of the “low-temperature structure” (i.e., the tetragonal one). The thermal stability of the sulfate to zirconium bond is in fact much higher than that of the hydroxyl bridges

(37) Widoniak, J.; Eiden-Assmann, S.; Maret, G. *J. Inorg. Chem.* **2005**, 3149–3155.

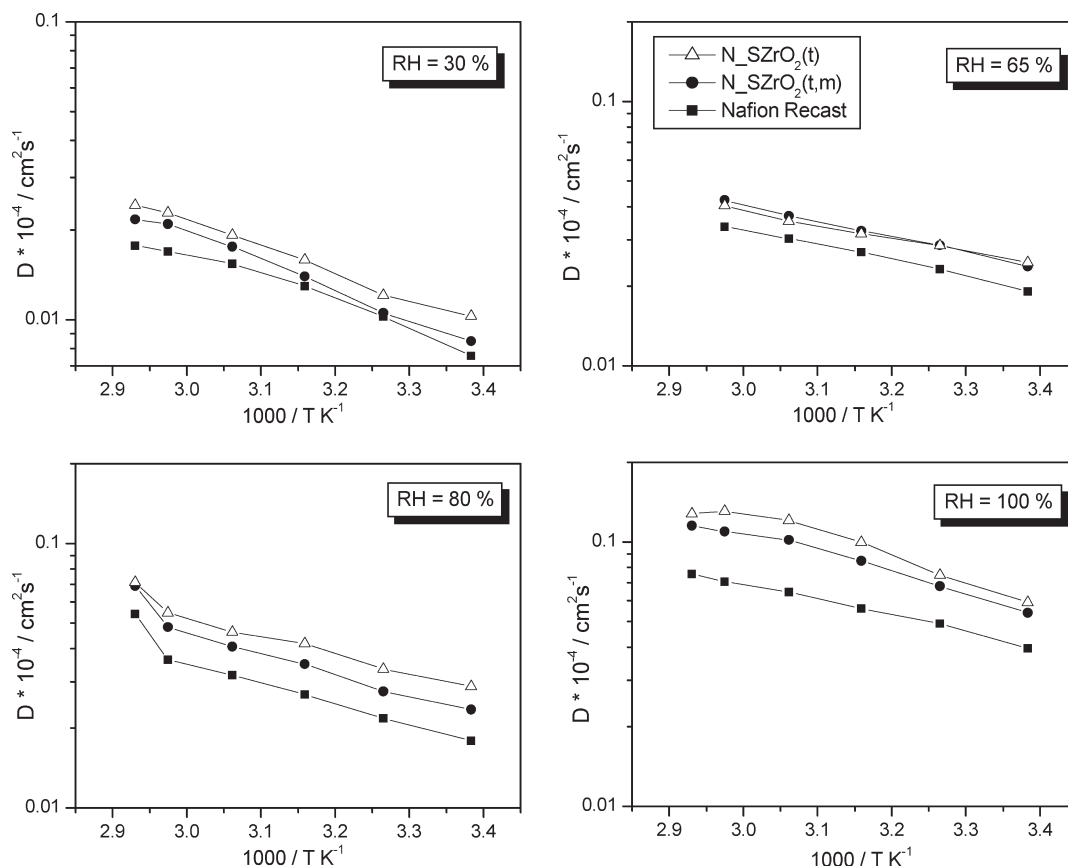


**Figure 9.** Self-diffusion coefficients of water ( $D_{\text{H}_2\text{O}}$ ) measured by PFGSE–NMR technique at different RH for N-SZrO<sub>2</sub>(t), N-SZrO<sub>2</sub>(t,m) and Nafion recast membranes, from 25 °C up to 80 °C.

across two Zr atoms, which delays the formation of some oxo bonds.<sup>36</sup>

Figure 7 displays the SEM micrographs of SZrO<sub>2</sub>(t,m) (Figure 7a) and SZrO<sub>2</sub>(t) (Figure 7b). The morphology consists of agglomerates of nanoparticles having an average diameter in the range 10–30 nm for both samples.

**3.2. Characterization of Composite Membranes.** Two composite Nafion-based membranes containing 5 wt. % of the two different sulfated zirconia samples (i.e., N-SZrO<sub>2</sub>(t,m) and N-SZrO<sub>2</sub>(t)) were prepared by a casting procedure together with a reference Nafion recast membrane. The ion exchange capacity values (IEC) measured for the three samples were quite similar, around 0.89 meq g<sup>-1</sup>, indicating an active contribution of the synthesized fillers in providing free acid groups to the membrane, as expected from the proton conductivity features of the sulfated oxide itself.<sup>26</sup>

Figure 8 shows the room temperature vapor phase water uptake (WU) behavior observed for Nafion recast and N-SZrO<sub>2</sub>(t,m) and N-SZrO<sub>2</sub>(t) composite membranes as a function of relative humidity (RH). The composites showed an enhanced WU when compared to Nafion in the whole range of RH investigated. The enhanced water uptake can be attributed to the hydrophilic nature of the additives within the pores of Nafion membrane.<sup>3</sup> This effect is particularly evident at low RH. In fact, the enhancement in WU is higher than 100% at 30% RH and only about 12.5% at 100% RH, for both

composites. In any case, WU values for the two doped membranes were similar, indicating that the different amount of SO<sub>4</sub><sup>2-</sup> groups on the zirconia surface (22 and 4% for the SZrO<sub>2</sub>(t) and SZrO<sub>2</sub>(t,m), respectively) does not strongly influence the room temperature water uptake.

PGSE-NMR experiments provide information on the translational motion of protons in the membrane by measurement of the water self-diffusion coefficients ( $D_{\text{H}_2\text{O}}$ ). By comparing the data relative to composite membranes having different amounts of sulfate groups bound to the inorganic additive the influence of surface modification on water retention and proton transport at different RH values and temperature can be evaluated. These data were then compared to those relative to Nafion recast measured under the same conditions. Figure 9 shows the Arrhenius plots of the water self-diffusion coefficients of Nafion recast and Nafion composite membranes at different RH values.  $D_{\text{H}_2\text{O}}$  values of the composite membranes were higher than those of unfilled Nafion in all RH conditions, in agreement with WU measurements, that is, higher water mobility is closely associated with higher water content<sup>38,39</sup>. However, although WU values of the two composite membranes were similar,  $D_{\text{H}_2\text{O}}$  of the N-SZrO<sub>2</sub>(t) was higher

(38) Nicotera, I.; Zhang, T.; Bocarsly, A.; Greenbaum, S. *J. Electrochem. Soc.* **2007**, *154*(5), B466–B473.

(39) Zawodzinski, T. A., Jr.; Neeman, M.; Sillerud, L.; Gottesfeld, S. *J. Phys. Chem.* **1991**, *95*, 6040–6044.

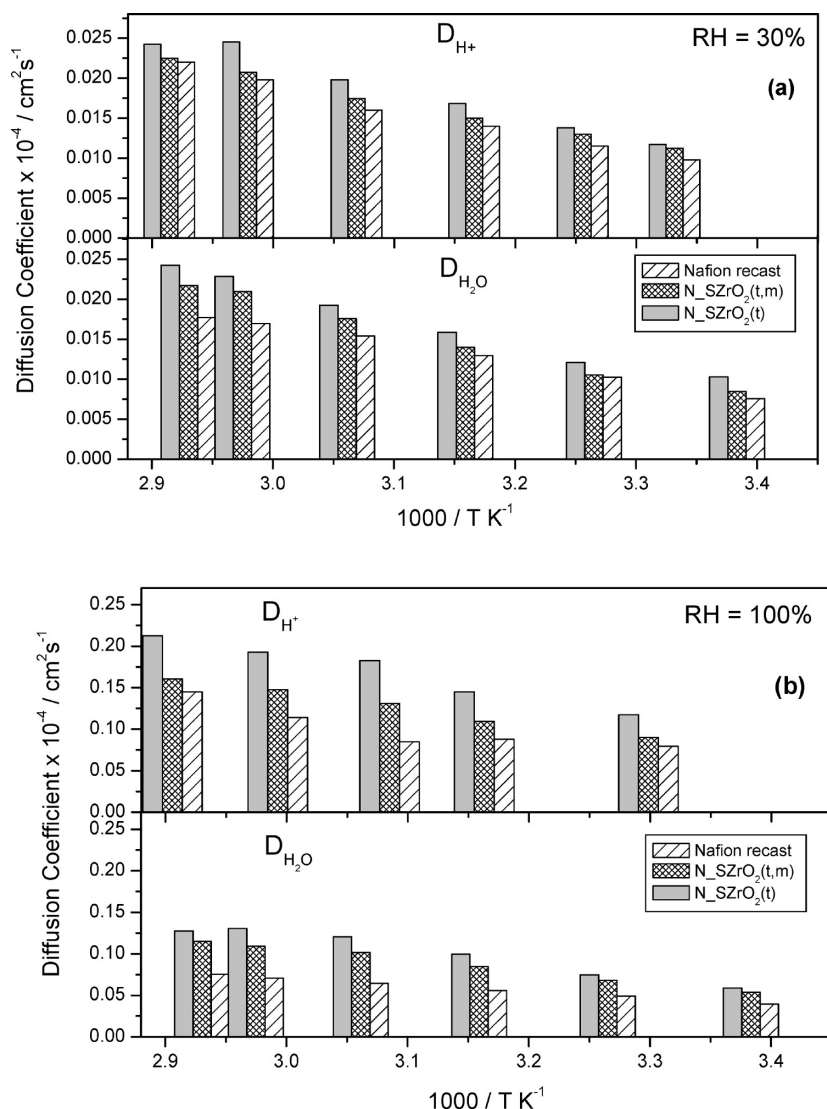


**Figure 10.** Comparison between proton diffusion coefficients ( $D_{H^+}$ ) derived by EIS and the self-diffusion coefficients of water ( $D_{H_2O}$ ) measured by NMR for N-SZrO<sub>2</sub>(t), N-SZrO<sub>2</sub>(t,m), and Nafion recast membranes at (a) 30% RH and (b) 100% RH.

than that of N\_SZrO<sub>2</sub>(t,m) in the whole range of RH and T examined. Given the similar hygroscopic character of the two membranes, the higher  $D_{H_2O}$  values measured for N\_SZrO<sub>2</sub>(t) cannot be a mere consequence of the extent of WU but must be due to the higher SO<sub>4</sub><sup>2-</sup> content of the SZrO<sub>2</sub>(t) filler that provided extra acid sites facilitating water diffusion.<sup>40</sup>

Proton conductivity ( $\sigma_{H^+}$ ) was measured by EIS and proton diffusivity ( $D_{H^+}$ ) was estimated from conductivity data using the Nernst–Einstein equation

$$D_{H^+} = \sigma_{H^+} \left( \frac{RT}{CF^2} \right) \quad (4)$$

where  $F$  is Faraday's constant,  $R$  is the universal gas constant,  $T$  is the absolute temperature, and  $C$  is the molar proton concentration that can be calculated from IEC and density values.  $D_{H^+}$  and  $D_{H_2O}$  values at 30% and 100% RH were evaluated as a function of temperature

and they are shown in panels a and b in Figure 10, respectively. The justification for their comparison is based on the simplified assumption that the average H<sup>+</sup> diffusion coefficient is approximately that of the water molecules on which they reside (even for a very short time on the NMR time scale), as in the case of an H<sub>3</sub>O<sup>+</sup> ion. Though eq 4's region of applicability is for much lower ion concentrations than in the present case, it still offers a convenient means to assess possible changes in conductivity mechanism. For all samples the mobility of protonic charge carriers and the water self-diffusion coefficients were similar at low RH, differing as the RH, hence water content, increased. At low RH values (Figure 10a), the difference between  $D_{H^+}$  and  $D_{H_2O}$  values was negligible, whereas at higher RH values (Figure 10b), such difference became larger. It is known that the difference between  $D_{H^+}$  and  $D_{H_2O}$  at high RH is due to the intermolecular proton transfer related to the mobility of protonic charge carriers (Grotthuss mechanism),<sup>41,42</sup>

(40) Ren, S.; Sun, G.; Li, C.; Song, S.; Xin, Q.; Yang, X. *J. Power Sources* **2006**, *157*, 724–726.

(41) Agmon, N. *Chem. Phys. Lett.* **1995**, *244*, 456.

(42) Kreuer, K. D. *Chem. Mater.* **1996**, *8*, 610.



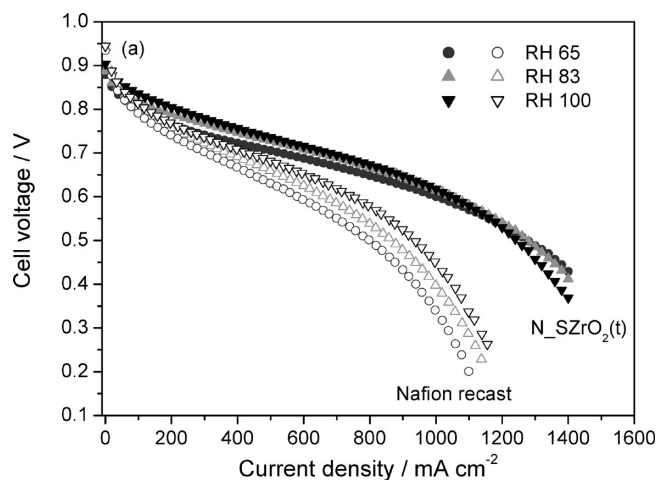


**Figure 11.** Polarization curves at 65, 83, and 100% RH values using MEAs fabricated with Nafion recast and N\_SrZrO<sub>2</sub>(t).  $P(\text{H}_2\text{-air}) = 2$  atm,  $T_{\text{cell}} = 70^\circ\text{C}$ .

indicating that transport of  $\text{H}^+$  by Grotthuss hopping becomes increasingly significant at high water contents, whereas it turned out to be negligible at low water contents.<sup>43</sup> Moreover, composite membranes showed enhanced  $D_{\text{H}^+}$  and  $D_{\text{H}_2\text{O}}$  values compared to those of unfilled Nafion. The increase in both  $D_{\text{H}_2\text{O}}$  and  $D_{\text{H}^+}$  of the N\_SrZrO<sub>2</sub> with respect to pure Nafion is the combined results of the enhanced water uptake as well as of the acidity. The sulfate groups on the zirconia surface introduce both acid Lewis sites and Bronsted acid sites, according to model proposed by Arata et al.,<sup>43,26</sup> with these sites facilitating both water self-diffusion coefficient and ionic mobility. It is noteworthy that the increased proton mobility at low RH values for N\_SrZrO<sub>2</sub> composites is a key point for their use in real fuel cell devices as electrolytes.

It is generally acknowledged that the performance of a PEMFC strongly depends on operative temperature, pressure and relative humidity. It is also well-known that low RH values allow to simplify the whole system and offer significant cost savings. For these reasons, we evaluated the influence of relative humidity on the PEMFC performances at a constant reference temperature (i.e.,  $70^\circ\text{C}$ ). Because of its attractive properties in terms of proton mobility and thermal stability, N\_SrZrO<sub>2</sub>(t) membrane was selected as electrolyte separator and tested in a  $\text{H}_2$ -air fuel cell.

Figure 11 shows the  $I$ - $V$  curves obtained with N\_SrZrO<sub>2</sub>(t) and unfilled Nafion membranes at  $70^\circ\text{C}$  and at different RH values, ranging from 65% to 100%. While the performance of the Nafion recast membrane was substantially affected by the humidity level, the polarization curves relative to the composite membrane showed only a small improvement with increasing RH from 65 to 100%.

Moreover, the polarization curves of the cells based on the composite membrane exhibited better characteristics than those based on Nafion recast in the same conditions:

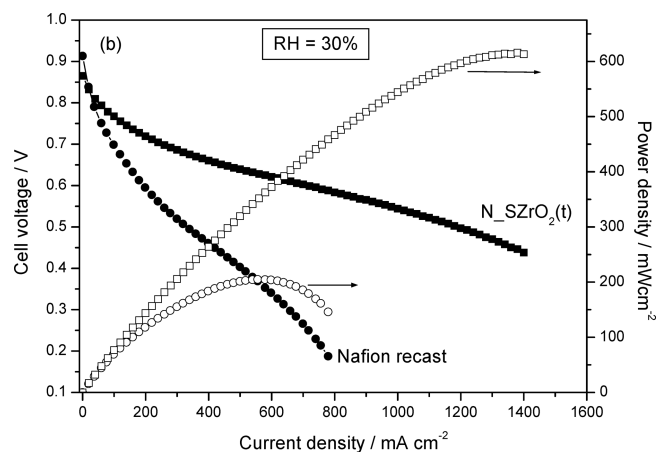


**Figure 12.** Polarization and power density curves at 30% RH using MEAs fabricated with Nafion recast and N\_SrZrO<sub>2</sub>(t).  $P(\text{H}_2\text{-air}) = 2$  atm,  $T_{\text{cell}} = 70^\circ\text{C}$ .

at 0.6 V and RH 83%, the current density for unfilled Nafion was  $680\text{ mA cm}^{-2}$ , whereas for the composite,  $1015\text{ mA cm}^{-2}$  was achieved. Moreover, it is interesting to note that in the low current density region the performance of Nafion recast and composite membranes were similar, whereas in the intermediate-high current density region, the differences between the two samples increased. This behavior can be ascribed to a low ohmic resistance and to an improved ion transport through the N\_SrZrO<sub>2</sub> membrane with respect to unfilled Nafion, according to NMR and EIS data.

Figure 12 shows the polarization and power density curves of N\_SrZrO<sub>2</sub>(t) and unfilled Nafion membranes at  $70^\circ\text{C}$  and at lower RH value, i.e., 30%. Again, the composite performed better than Nafion but the difference between the two samples in terms of current (and power) density is higher with respect to the higher RH cases shown in Figure 11, in fact at 0.6 V the current density for unfilled Nafion was only  $200\text{ mA cm}^{-2}$ , whereas for the composite,  $930\text{ mA cm}^{-2}$  was achieved. This enhancement corresponds to a 200% increase of in terms of power density. Furthermore, differently from the high RH case (Figure 11), at lower RH the N\_SrZrO<sub>2</sub>(t) membrane showed a much higher performance than that of Nafion both in the activation and in the ohmic-diffusion control region. This behavior can be ascribed to an enhanced membrane-electrode interface contact, probably because of the absence of ionomer shrinkage,<sup>29</sup> as well as to a lower mass-transport limitation. These findings indicate that the filler effect is more evident at low RH.

#### 4. Conclusions

Synthesis parameters, adopted during the preparation of sulfated zirconia particles, were found to play a key role in the properties of the resulting powders. Crystallographic form, as well as sulfate group concentration, was strongly influenced by the thermal treatments chosen for the formation of the oxide precursor. In any case, hydrothermally stable compounds were obtained, as the

(43) Arata, K.; Hino, M. *Appl. Catal., A* **1990**, *59*, 197.



sulfate groups tightly bonded to Zr on a heat-treated  $\text{SZrO}_2$  surface.

The positive effect of the synthesized sulfated zirconia on Nafion properties was demonstrated. The superacidic inorganic compound promoted higher hydration level in the composite membranes with respect to an additive-free Nafion membrane, as revealed by water uptake measurements.

The presence of the inorganic compound resulted also in higher water diffusion coefficients for the doped membranes over a wide range of temperature (i.e., 25–90 °C) and external relative humidity (i.e., 30–100%). In particular,  $\text{SZrO}_2(\text{t})$ , by virtue of its greater amount of surface  $\text{SO}_4^{2-}$ , allowed the best water diffusivity among those related to the samples here investigated.

Proton conductivity, as derived from impedance spectroscopy measurements, was used to calculate proton diffusion coefficients using the Nernst–Einstein equation. For all samples,  $D_{\text{H}^+}$  values were much higher than water self-diffusion coefficients at 100% RH in the whole range of explored temperatures, while there were no big differences between  $D_{\text{H}^+}$  and  $D_{\text{H}_2\text{O}}$  at 30% RH. This reveals that the intermolecular proton transfer, related to the mobility of protonic charge carriers, becomes significant at high water contents. In any case, the composite membranes exhibited an improved proton and water diffusivity with respect to undoped Nafion, also at a very low hydration level.

$\text{SZrO}_2(\text{t})/\text{Nafion}$  membrane was used as electrolyte separator in a fuel cell working at 70 °C in the range 30–100% RH. Interestingly, the performances of the cell,

in terms of current and power delivered, were almost independent of the relative humidity level. In comparison with an unmodified Nafion-based cell, the greatest enhancement was found by using the composite membrane electrolyte at 30% RH. This result is very attractive in view of potential application in fuel cells for transportation. Here, in fact, the cell stack must be able to perform without external humidification, which is a source of additional cost and complexity to the system. A further and more detailed analysis of the cell performances, using the synthesized sulfated zirconia particles as both membrane and electrode additives, is currently being developed in our laboratories, by exploring a wide range of operating conditions.

**Acknowledgment.** Part of this work has been performed in the framework of the NUME Project, titled “Development of composite proton membranes and of innovative electrode configurations for polymer electrolyte membrane fuel cells” supported by the Italian Ministry of University and Research, MIUR, program FISR 2001. The financial support of the Ministry for Foreign Affairs (Italy-Quebec Joint Lab for Advanced Nanostructured Materials for Energy, Catalysis and Biomedical Applications) is also gratefully acknowledged. FIRB, Project “RINNOVA” titled “Innovative electrochemical technologies for energy storage from renewable sources”, is sponsored by the Italian Ministry of University and Research. The work at Hunter College was supported by a grant from the U.S. Air Force Office of Scientific Research and the National Institutes of Health through the RCMI (RR003037) MBRS-RISE programs.